Membrane matters: The impact of a nanodisc-bilayer or a detergent microenvironment on the properties of eubacterial rhodopsins

Ganapathy, S.; Opdam, L.V.; Hontani, Y.; Frehan, S.; Chen, Q.; Hellingwerf, K.J.; ... ; Grip, W.J. de

BBA - Biomembranes 1862 (2020) 183113

Contents lists available at ScienceDirect

BBA - Biomembranes

journal homepage: www.elsevier.com/locate/bbamem

Membrane matters: The impact of a nanodisc-bilayer or a detergent microenvironment on the properties of two eubacterial rhodopsins

Srividya Ganapathy[a,*], Laura Opdam[a], Yusaku Hontani[b], Sean Frehan[b], Que Chen[c], Klaas J. Hellingwerf[c], Huub J.M. de Groot[a], John T.M. Kennis[b], Willem J. de Grip[a,d,**]

[a] Department of Biophysical Organic Chemsitry, Leiden Institute of Chemistry, Leiden University, Leiden, the Netherlands
[b] Department of Physics and Astronomy, VU University Amsterdam, Amsterdam, the Netherlands
[c] Swammerdam Institute for Life Sciences, University of Amsterdam, Amsterdam, the Netherlands
[d] Department of Biochemistry, Radboud University Medical Center, Nijmegen, the Netherlands

ARTICLE INFO

Keywords:
Microbial rhodopsins
Membrane proteins
Detergent micelles
Nanodisc
Thermal stability
Photoresponse

ABSTRACT

Multi-spanning membrane proteins usually require solubilization to allow proper purification and characterization, which generally impairs their structural and functional integrity. We have tested the efficacy of several commonly used detergents and membrane-mimicking nanodiscs with respect to solubilization, spectral properties, thermal stability and oligomeric profile of two membrane proteins from the eubacterial rhodopsin family, green proteorhodopsin (PR) and *Gloeobacter violaceus* rhodopsin (GR). Good solubilization was observed for the detergents TritonX-100 and dodecylphosphocholine (DPC), but DPC in particular strongly affected the thermal stability of PR and especially GR. The least deleterious effects were obtained with n-dodecyl-β-D-maltopyranoside (DDM) and octyl glucose neopentyl glycol (OGNG), which adequately stabilized the native oligomeric and monomeric state of PR and GR, respectively. The transition from the oligomeric to the monomeric state is accompanied by a small red-shift. Both GR and PR were rather unstable in SMA-nanodiscs, but the highest thermal stability was realized by the MSP-nanodisc environment. The size of the MSP-nanodisc was too small to fit the PR hexamer, but large enough to contain the PR monomer and GR trimer. This permitted the comparison of the photocycle of trimeric GR in a membrane-mimicking (MSP-nanodisc) and a detergent (DDM) environment. The ultrarapid early phase of the photocycle (femto- to picosecond lifetimes) showed very similar kinetics in either environment, but the slower part, initiated with proton transfer and generation of the M intermediate, proceeded faster in the nanodisc environment. The implications of our results for the biophysical characterization of PR and GR are discussed.

1. Introduction

Membrane proteins containing multiple membrane spanning domains are insoluble in aqueous solution, which presents a major drawback in their structural and functional characterization. Usually this characterization requires solubilization by amphipathic agents for the extraction of such proteins from the membrane, and subsequent purification. Solubilization into detergent micelles is the most popular method for this purpose and is particularly useful for initial biophysical characterization of membrane proteins. Detergent micelles contain a hydrophobic interior and hydrophilic exterior and yield soluble protein-detergent complexes when associated with membrane proteins, which share this amphipathic nature. A wide variety of detergents exist with different combinations of head and tail groups [1]. The size of the protein-detergent complexes usually depends on the polar headgroup of the detergent. However, the detergent shell is usually not able to sustain the structural stability and functional activity of a membrane protein to the same extent as the native lipid micro-environment [1–3]. Hence, it is a challenge to select a suitable detergent to properly solubilize and stabilize a particular membrane protein, both because of the poorly defined properties of protein-detergent complexes and because of the individual demands of a selected protein. The mild detergent n-dodecyl-

Abbreviations: PR, green absorbing proteorhodopsin from Monterey Bay; GR, *Gloeobacter violaceus* rhodopsin; DDM, n-dodecyl-β-D-maltopyranoside; DPC, dodecyl phosphocholine; MSP, membrane scaffold protein; SMA, styrene maleic acid copolymer; OG, n-octyl-β-D-glucopyranoside; OGNG, octyl glucose neopentyl glycol; MOA2, all-*trans* 3-methoxy retinal A2; A1, all-*trans* retinal A1; CD, circular dichroism; SEC, size exclusion chromatography

* Correspondence to: S. Ganapathy, Department of Imaging Physics, Delft University of Technology, Delft, the Netherlands.
** Correspondence to: W.J. de Grip, Department of Biochemistry, Radboud University Medical Center, Nijmegen, the Netherlands.
E-mail addresses: S.Ganapathy-1@tudelft.nl (S. Ganapathy), w.j.de.grip@umail.leidenuniv.nl (W.J. de Grip).

https://doi.org/10.1016/j.bbamem.2019.183113
Received 5 July 2019; Received in revised form 20 October 2019; Accepted 22 October 2019
Available online 28 October 2019

β-D-maltopyranoside (DDM) is the most widely used detergent for solubilization of membrane proteins, since it has relatively minor deleterious effects on the structure and stability of most membrane proteins [1,3–5].

Micellar systems are preferable over membrane-bound systems for studying the photophysical properties of colored membrane proteins, since they cause relatively little light-scattering. However, proteins are dynamic structures, and in addition usually undergo functional conformational changes like the opening and closing of channels. The loss of protein-lipid and lipid-lipid interactions makes these proteins vulnerable to destabilization in the micellar environment, especially in studies involving protein- or chromophore engineering, which often will render a protein more sensitive to structural perturbation. The lateral pressure induced by the membrane lipid bilayer has a stabilizing influence on membrane proteins [6]. Therefore a number of systems have been devised which simulate the membrane environment of these proteins. Various phospholipid bilayer systems, such as proteoliposomes and nanodiscs, have become very popular for the stabilization of membrane proteins, which allows one to study their properties in a native-like environment [1–3,7–9].

Proteoliposomes are commonly used for the study of vectorial processes, and for the solid-state NMR investigation of protein structure [8,10]. However, due to the light scattering induced by their large size (200 nm-10 μm diameter), they are less suitable for optical studies. The much smaller discoid open nanodisc systems (10–30 nm diameter) are a suitable alternative, due to their optical near-transparency. Nanodiscs consist of the protein of interest, embedded in a phospholipid bilayer, contained by a scaffolding amphipathic agent (Fig. 1). Traditionally, nanodiscs are prepared using two molecules of an amphipathic membrane scaffold protein (MSP) [11]. These nanodiscs are usually 9–20 nm wide, with the diameter of the nanodisc being controlled by the length of the particular MSP used [7]. However, these MSP-nanodiscs require prior detergent solubilization of the pigment, which then allows subsequent insertion of the solubilized protein into a non-native membrane environment, although detergent exposure can be minimized, while (partially) retaining native lipids [12,13]. SMA-nanodiscs, composed of a styrene maleic acid copolymer as a scaffolding component, are an alternative emerging option which allows detergent-free insertion of membrane proteins into nanodisc structures [14]. SMA self-inserts into the cell membrane, thereby extracting native-nanodisc patches, which can be further purified to isolate the nanodiscs embedding the protein of interest.

Here, we investigate the effect of the local micellar or membrane microenvironment on the properties of two model membrane proteins, namely green absorbing proteorhodopsin (PR, λ_{max} 520 nm) [15] and *Gloeobacter violaceus* rhodopsin (GR, λ_{max} 540 nm) [16]. These proteins are archetypes of the eubacterial rhodopsin family of proton-pumps, orthologous to the well-studied archaeal bacteriorhodopsin (bR), but differ in their functional oligomeric state (penta-and hexamers for PR, trimers for GR). Proteorhodopsin was first discovered in 2000 during a metagenomic screen of marine uncultured gamma-proteobacteria from Monterey Bay in California [15]. Since then, several variants of PR have been found, widely distributed in diverse organisms across the photic zone, making them a hot topic of current research [17]. On the other hand, GR, which was isolated from a thylakoid-less cyanobacterium [16], has been studied much less extensively.

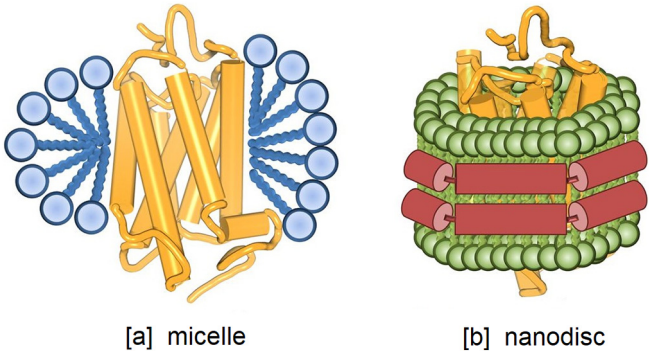

Fig. 1. Schematic representation of the microenvironments for membrane proteins, which have been investigated in this study, after their extraction from their biological membranes, adapted from Milic et al. [70]. Detergent molecules are represented in blue, lipids in green, the intrinsic membrane protein in yellow and membrane scaffold components in red. The size of the micelle depends on many factors, like the size of the membrane protein, pH, ionic strength, etc.

PR and GR bind a molecule of all-*trans* retinal as a chromophore and function as light-driven proton pumps. They contain the typical seven-membered α-helical bundle motif (called opsin) common to a large number of membrane proteins. Both PR and GR show excellent expression in the Gram-negative bacterium *Escherichia coli*, which is a very popular host for inducible expression of membrane proteins, due to its rapid growth, high transformation efficiency and well-characterized and extensive genetic toolbox. Biophysical characterization of these pigments requires extraction from the *E. coli* membrane with a detergent, such as DDM, and subsequent purification. If required, they can thereupon be embedded into an artificial membrane environment, e.g. in the form of proteoliposomes or nanodiscs [1,4,7,18].

In this study, we compare a number of detergent systems and study their influence on the spectral properties, stability, size and oligomeric state of the resulting PR and GR protein-detergent complexes, to investigate infiltrative detergent effects. These systems are further compared to the corresponding nanodisc phospholipid bilayer systems, generated using SMA (native lipid nanodiscs) and MSP (non-native lipid nanodiscs) (Fig. 1). Finally, we compare the photocycle of GR in a detergent and nanodisc environment using transient absorption spectroscopy. Overall, the least deleterious effects were observed for the detergents DDM and octyl glucose neopentyl glycol (OGNG). For spectroscopic studies in a native-like state DDM is most appropriate for PR, while a MSP-nanodisc-bilayer environment can be recommended for GR.

2. Materials and methods

2.1. Materials

Sources of special chemicals: 1,4-Dithiothreitol (DTT) and Benzonase nuclease (Novagen); octyl-β-D-glucopyranoside (OG), TritonX-100, HEPES, heptakis-2,6-di-*O*-methyl-β-cyclodextrin, lysozyme, asolectin (Sigma-Aldrich); SMA 2000 (Cray valley); 1-n-dodecyl-β-D maltopyranoside (DDM), octyl glucose neopentyl glycol (OGNG) (Anatrace); MSP1E3D1-plasmid (Addgene); *E. coli* polar lipid extract (Avanti polar lipids); Ni^{2+}-NTA resin and Coomassie Brilliant-blue G (Thermo-Scientific Fischer); EDTA-free protease inhibitor cocktail (Roche); all-*trans*-3-methoxy-3,4-dehydroretinal (MOA2, Buchem B.V.) All other chemicals were of analytical grade.

2.2. Cell lines, plasmids, and cell culturing

E. coli UT5600 was transformed with the pKJ900 plasmids, encoding PR or GR with a C-terminal 6×-His tag [19]. A main culture was grown from a 1:50 dilution of an overnight culture in LB at 37 °C. Expression of the opsin was induced with 0.5 mM IPTG at an OD_{600} of 0.5–0.6. The cells were grown for an additional 14–16 h, and harvested by centrifugation at 3200 ×*g* for 20 min at room temperature (RT). *E. coli* BL21 was used to express the plasmid pET-28a, containing an insert for the 6× His-tagged membrane scaffold protein MSP1E3D1 [11]. A main culture was grown from a 1:50 dilution of an overnight culture in Terrific broth at 37 °C. Expression of MSP1E3D1 was induced using 0.5 mM IPTG at an OD_{600} of 0.6–0.7. The cells were grown for an additional 2–4 h and harvested by centrifugation at 3200 ×*g* for 20 min at

RT.

2.3. Hydrolysis of SMA

This procedure was adopted from Dörr et al. [14]. 10 g of styrene maleic acid copolymer SMA2000 was refluxed in 100 mL 1 M KOH for 3 h at 100 °C. The solution was cooled to RT and kept at 4 °C overnight. The hydrolyzed SMA was precipitated with 1 M HCl, by lowering the pH to 7. SMA was spun down in a tabletop centrifuge at 6000 ×*g* for 20 min, and the pellet was further washed 4 to 5 times with 100 mM HCl. The supernatant was drained and the solid precipitate was lyophilized overnight. From the refluxed solution, 98% of SMA was recovered. A stock solution of 10% SMA (*w/v*) was made in 50 mM Tris, pH 8.

2.4. Extraction of PR and GR into SMA-nanodiscs

Cell pellets of *E. coli* UT5600 s expressing PR or GR were resuspended in 50 mM Tris, 0.6 M NaCl, pH 8 (3 mL per pellet of a 100 mL culture), and were sonicated to generate membrane vesicles (4 s on, 5 s off, 30% amplitude, 10 min, 4 °C). 3 mL of 10% SMA was added and the solution was sonicated again and left on a roller at RT for 2–3 days. The insoluble fraction was spun down at 147,000 ×*g* for 45 min at 4 °C. From the colored supernatant, PR or GR containing SMA-nanodiscs were purified using nickel affinity chromatography.

2.5. Purification of MSP1E3D1

The *E. coli* BL21 cell pellet was resuspended in 40 mM Tris, 0.3 M NaCl, 5 mM β-mercaptoethanol, pH 8 (10 mL per L culture), supplemented with one protease inhibitor tablet, 10 mg lysozyme and 6 μL benzonase nuclease solution. After 30 min incubation on ice, 250 μL of 10% Tergitol NP-40 was added and the pellet was sonicated 5 times, 45 s, 30% amplitude, 4 °C. The cell debris was spun down at 16,000 ×*g* for 30 min at 4 °C. The lysate was subjected to batch purification using 6 mL Ni^{2+}-NTA resin, as described previously [20]. The fractions with pure MSP1E3D1 were combined and concentrated using a 10 kDa centrifugal filter (Amicon). The purity was assessed using SDS-PAGE. A major band at ~30 kDa represents MSP1E3D1. A weak band beneath the main MSP band represents a truncated form of the MSP that also participates in nanodisc formation [20].

2.6. Purification of pigment-detergent complexes

These procedures were adapted from our previous papers [21, 22]. A pellet of *E. coli* cells expressing the PR or GR opsin was resuspended in ice cold lysis buffer (5 mL/100 mL culture volume) containing 20 mM Tris, 50 mM NaCl, 20 mM imidazole, 0.1% DDM, pH 7, supplemented with an EDTA-free protease inhibitor tablet, benzonase (4 units/100 mL culture) and lysozyme (4 mg/100 mL culture). The suspension was sonicated at 4 °C and centrifuged to remove cellular debris. At this stage, the crude mixture was incubated with 20 μM retinal A1 or its analog MOA2 for 1 h at RT. Detergent was then added to a final concentration of either 4% DDM (*w/v*), 2.5% DPC (w/v), 2.5% OG (w/v) or 5% Triton-X100 (*v*/v). The samples were kept rotating for 1–3 days at 4 °C or RT. The insoluble material was removed by centrifugation (20,000 ×*g*, 20 min, 4 °C). The His-tagged rhodopsins were purified using immobilized-metal affinity chromatography (IMAC) with 0.4 mL Ni^{2+}-NTA resin per 100 mL original culture volume. All the solutions used during purification contained 0.1% of the detergent of choice, except for OGNG which was used at 0.5%. The resin was contained in a spin column and first equilibrated with buffer A (20 mM bis-tris propane, 0.5 M NaCl, 0.1% detergent, pH 8) containing 20 mM imidazole. The crude extract was allowed to equilibrate with the column for 15 min at RT. The column was washed 5 times with 5 column volumes of buffer A containing 50 mM imidazole at RT. Finally, strongly bound protein was eluted using buffer A containing 500 mM imidazole at RT. Fractions containing purified pigment were combined and concentrated using a 10 kDa cut-off column (Amicon) and analyzed by spectroscopy and SDS-PAGE. Due to the poor solubilization efficiency of OGNG, samples were first solubilized and bound to the Ni^{2+} NTA -resin in 4% DDM and subsequently washed and eluted with 0.5% OGNG.

2.7. Formation of MSP-nanodiscs

PR and GR, solubilized and purified in DDM, were used to generate MSP-nanodiscs. A solution of 2 mg/mL asolectin or *E. coli* polar lipid was made in 40 mM nonylglucose, 50 mM HEPES, 100 mM NaCl, pH 7.8. The entire protocol was carried out at 4 °C with continuous mixing in the incubation steps. Purified PR or GR was combined with the lipid solution at a molar ratio of 1:120 for pigment:asolectin or *E. coli* lipid. This mixture was incubated for 30 min. Then MSP1E3D1 was added in a molar ratio of 2:1 to PR or GR. The solution was vortexed and incubated for 30 min. Subsequently, DDM was extracted from the mixed micelles complexed by the addition of β-cyclodextrin, which forms inclusion-complexes with DDM [17]. This induces the formation of the MSP-nanodiscs [18]. β-cyclodextrin was added in three equal parts, with 15 min incubation steps after each addition, to achieve a final molar ratio of 1:1.5 for detergent:β-cyclodextrin. Any insoluble material was then spun down at 14,000 ×*g* for 30 min at 4 °C.

2.8. Purification of SMA- and MSP-nanodiscs

The SMA- and MSP-nanodiscs containing PR or GR were purified by nickel-affinity chromatography. 0.3 or 1 mL Ni^{2+} NTA-resin in 0.6 or 5 mL columns was spun down in a table top centrifuge at 2700 ×*g* for 1 min and washed once with Buffer A (20 mM bis-tris propane, 20 mM imidazole, 0.5 M NaCl, pH 8). The crude nanodisc solution was added to the column, incubated at RT for 20 min, and the unbound lysate was removed by centrifugation. The columns were washed ten times with 0.6 mL of Buffer A. The bound nanodiscs were eluted using 600 μL of 500 mM imidazole, 20 mM bis-tris propane, 0.5 M NaCl, pH 8. The purified nanodiscs were concentrated using a 10 kDa cut-off column (Amicon) to a final buffer concentration of 20 mM bis-trispropane, 150 mM NaCl, pH 8. Absorbance spectra of the purified nanodiscs were recorded, and their purity was assessed by SDS-PAGE as described previously [21,22].

2.9. UV–Vis spectroscopy

The spectral properties of all purified pigment-detergent and pigment-nanodisc samples were measured using a Shimadzu UV–Vis spectrophotometer (UV-1601) as described previously [21,22]. The absorbance maxima were determined using the internal peak-pick function of the software UVProbe.

2.10. Size exclusion chromatography

Size exclusion chromatography (SEC) of purified PR/GR in DDM or OGNG was done using a mobile phase containing 50 mM phosphate buffer, 150 mM NaCl, 0.2% OGNG, pH 8 or 20 mM bis-tris propane, 150 mM NaCl, 0.1% DDM, pH 8 with a 10 μL injection loop on a SuperdexTM 200 Increase 5/150 GL column (GE Healthcare) at standard pressure and flow rate. The absorbance of the eluate was measured at 215, 280 nm, 500 nm, 520 nm and 540 nm. Blue Dextran (Sigma-Aldrich) was used for determining the void volume. A set of soluble proteins with known molecular weights was used to calibrate the column (see Fig. S4, Supporting Information).

2.11. Circular dichroism spectroscopy

Circular dichroism (CD) spectra were recorded using 2 mm quartz

cuvettes on a J-815 spectrometer (Jasco, Gross-Umstadt, Germany) equipped with temperature control. The following parameter settings were used: wavelength range, 400–900 nm; data pitch, 1 nm; response time, 2 s; band width, 4 nm; scanning speed, 50 nm/min; temperature, 20 °C. A sample absorbance of 0.5–1 OD units at the λ_{max} was used throughout.

2.12. Dynamic light scattering

The size distribution of detergent micelles and purified nanodisc samples was analyzed using the Zetasizer Nano-S (Malvern Instruments Ltd., Malvern UK), equipped with a 633 nm laser. The OD at the λ_{max} of the samples was adjusted to 0.5–1 OD units in a final concentration of 2–2.5% of the detergent of choice. The samples were spun in a table-top centrifuge at 13,000 $\times g$ for 10 min prior to the measurement, to remove dust particles. The signals were analyzed using the internal software of the equipment and converted into a size distribution with scatter intensity.

2.13. Transient spectroscopy

Transient absorption measurements were performed using a femtosecond to sub-millisecond pump-probe setup as described previously [23–25]. A 2-mm thick CaF_2 plate was used for supercontinuum white light generation, and a selected wavelength region; 380–670 nm, was detected by the photodiode array. The transient absorption data was acquired within a time window from −50 ps to 300 µs, relative to the arrival time of the pump pulse at the sample position, with a minimum temporal step of 50 fs. The diameter of the pump and the probe beams at the sample position were ~200 µm and ~70 µm, respectively. The wavelength of the pump beam was centered at 570 nm (GR:A1; DDM), 520 nm (GR:A1; MSP-nanodisc), 480 nm (GR:MOA2; DDM) or 620 nm (GR:MOA2; MSP-nanodisc). Global analysis was performed using the Glotaran programme as described previously [23,26]. The standard errors of the time constants on the global fitting were < 10%.

3. Results

3.1. Selection of detergents and purification of pigments

We compared the effect of several different detergent environments on the spectral properties and stability of PR and GR (Fig. 2). The mild nonionic detergent n-dodecyl-β-D-maltopyranoside (DDM) is the most commonly used detergent to solubilize membrane proteins. Besides this detergent, we also included the non-ionic detergents TritonX-100 and n-octyl-β-D-glucopyranoside (OG), which are members of the polyoxyethylene and acylsaccharide class, respectively; both are more aggressive than DDM. In addition, we included octyl glucose neopentyl glycol (OGNG), which has only recently become available. OGNG has similar stabilization potential as DDM [27]. Finally, we included the zwitterionic detergent dodecyl phosphocholine (DPC), which is commonly used to investigate membrane proteins with liquid-state NMR, since it generates relatively small mixed micelles (Table 1) [28].

Membrane vesicles, containing the C-terminally 6xHis tagged PR or GR, were isolated from the *E. coli* UT5600 cells, and solubilized using 2.5–5% (*w/v*) of the detergent of choice as described previously [22]. The pigments were subsequently purified by exploiting the his-tag and concentrated to a final detergent concentration of 2%. The exception to this was OGNG, which turned out to perform very poorly in directly extracting the pigments from the membrane vesicles. In this case, the pigments were first dissolved in 4% DDM, bound to the Ni^{2+}-affinity column and washed and eluted with 0.5% OGNG.

Table 1
Absorbance maximum of PR and GR in different detergent environments.

Detergent	Mol. weight[a]	cmc[b] (mM)	conc[c] (mM)	Diameter[d] (nm)	λ_{max}[e] PR (nm)	λ_{max}[e] GR (nm)
DDM	510.6	0.16	40	5.4	520	540
DPC	351.3	1.1	57	3.6	522	537
TritonX-100	~625	~1	31	6.4	521	541
OG	292.4	20	65	4.3	527	545
OGNG	568.7	~1	35	nd	531	553

[a] Molecular weight of the detergents in g·mol^{-1}.
[b] Critical micelle concentration (from deGrip et al. [4] for DDM or provided by the manufacturer).
[c] Detergent concentration used in this experiment.
[d] Average diameter of detergent micelle determined by DLS, accuracy ± 1 nm. nd = not determined
[e] λ_{max} value of purified pigment at pH 8, accuracy ± 2 nm.

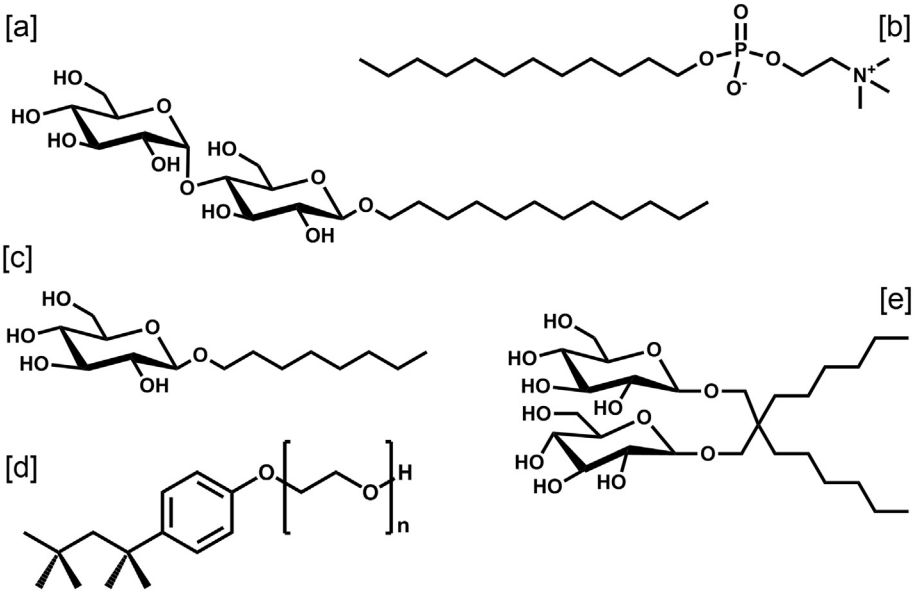

Fig. 2. Chemical structure of detergents used in this study to solubilize and/or purify the pigments. DDM [a], DPC [b], OG [c], TritonX-100, n = 9–10 [d] and OGNG [e]. See Materials and methods for full chemical names.

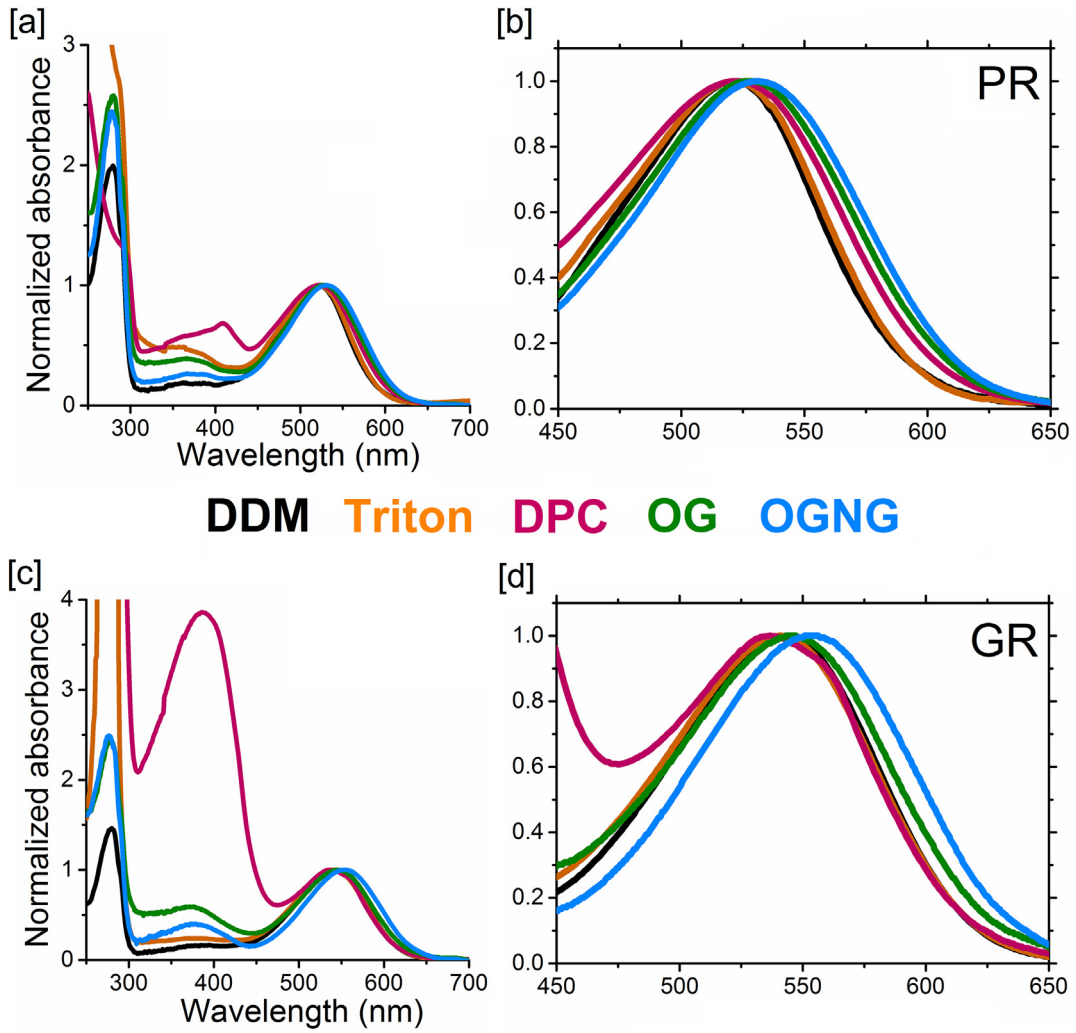

Fig. 3. Absorbance spectra of PR [a,b] and GR [c,d] recorded immediately after purification in various detergent environments at pH 8 and RT, normalized at the main visible absorbance band of the intact pigment. Color codes are as shown by the detergent abbreviations in the figure.

3.2. Effect of the detergent environment on stability, spectral properties and oligomeric state of PR and GR

The thermal stability of the purified pigments was assessed by following the decay of the main absorbance band at pH 8 at the commonly used temperatures for characterization of proteins of 4 °C and RT (c.f. Fig. 3). Although membrane proteins usually are more stable at low detergent concentrations (< 0.2%), we used a 2% concentration to aggrandize the differences in stabilizing faculty between the detergents and did not measure exact half-lives. DPC was found to be the most destabilizing detergent. Even upon short solubilization, like for 1 h at 4 °C, followed by rapid purification, a band was clearly observed around 390 nm in the absorbance spectrum of the purified protein (Fig. 3). This band most likely represents retinal released from denatured pigment. The destabilization was very pronounced for GR (Fig. 3C). The most efficient solubilization was obtained with TritonX-100, which required 1 h solubilization at RT (or overnight at 4 °C). The purified PR samples were stable at 4 °C for 3 to 4 days in this detergent before slow loss of the typical absorbance band was detectable. However, GR purified in TritonX-100 was less stable. It did not survive 2 h incubation at RT, or a week of storage at 4 °C, nor repeated freeze-thaw cycles. OG required considerably longer (e.g. overnight) incubation at RT for complete solubilization, but showed similar results to TritonX-100 in terms of thermal stability of the purified pigments. Complete solubilization with DDM required 2–3 days at RT. The resulting purified pigments showed the highest stability and could be stored in DDM at RT for at least a week without detectable loss of pigment. The poorest solubilization efficiency was seen for OGNG, which achieved < 10% solubilization of the pigments after a week of extraction at RT. However, the pigments obtained upon purification in OGNG, were stable at RT for at least a week, quite comparable to DDM.

Solubilization with TritonX-100, DPC and DDM results in about the same absorbance maximum for either pigment (Table 1). However, both OG and OGNG cause a significant red-shift in the λ_{max} of PR as well as GR (5–13 nm). In view of the stability of the pigments in OGNG and their red shifted absorbance, we investigated their oligomeric status using SEC and CD. From the size exclusion pattern (Fig. 4, top panels), we conclude that OGNG micelles contain a relatively uniform population of monomeric PR and GR. In agreement with literature data DDM micelles maintain a relatively uniform population of trimeric GR and mainly larger oligomers of PR [29–33]. The bilobal CD spectrum for PR and GR in DDM (Fig. 4, panel c) is in agreement with an ordered oligomeric state, since it implies close-range communication between the retinylidene ligands of the subunits [34,35]. The CD spectrum of PR and GR in OGNG only shows low amplitude peaks and has lost most of this bilobal character. (Fig. 4, panel d), which would agree with a mainly monomeric state [30].

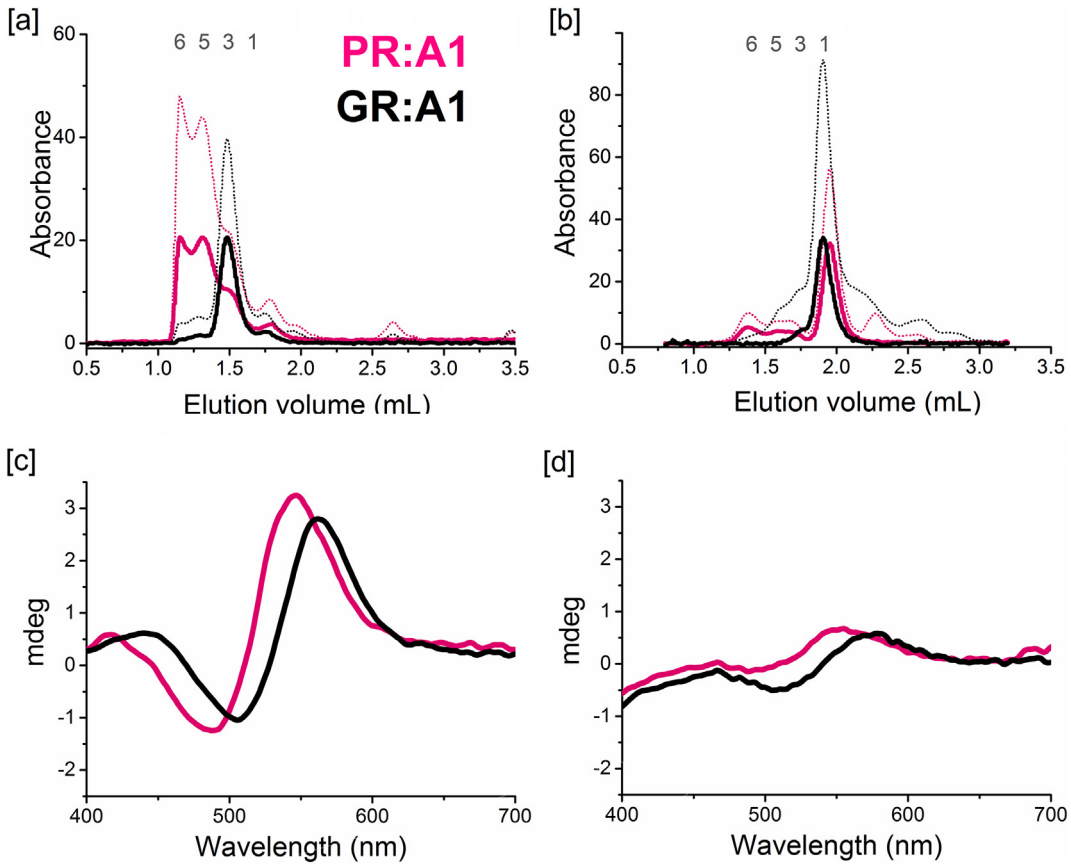

Fig. 4. Top panel: SEC chromatograms of PR (pink) and GR (black) at pH 8 in 0.2% DDM [a] or 0.2% OGNG [b]. Dotted line, absorbance at 280 nm; solid line, absorbance ~500 nm. Bottom panel: Circular dichroism spectra in 2% DDM [c] or 2% OGNG [d]. A1 stands for pigments with the native chromophore (retinal A1). The absorbance scale on the y-axis in panels a and b is presented in mOD. Calibration with soluble proteins and the resulting molecular weights of the bands in panels a and b are presented in the supporting information (Fig. S4).

3.3. Formation and characterization of nanodisc-protein complexes

PR and GR purified in DDM were used to generate MSP-nanodiscs. The phospholipid mixture from soybean (asolectin), and *E. coli* (polar extract) were both tested as suitable lipid environments and yielded similar results. The purified pigment was mixed with lipid and MSPDE31 in a defined ratio, after which the detergent was extracted with β-cyclodextrin [18]. This extraction step concomitantly cajoles the assembly of MSP-nanodisc. The MSP-nanodiscs were purified from the cyclodextrin inclusion mixture by nickel affinity chromatography, exploiting the 6xHis tag on the opsin and the MSP. The purified MSP-nanodiscs were characterized using absorbance spectroscopy, SDS-PAGE and dynamic light scattering (DLS).

The yield of pigment MSP-nanodiscs generated with purified PR (~10% insertion of pigment) was consistently substantially lower than that obtained with GR (~95% insertion). Furthermore, in contrast to GR the absorbance band of the PR:MSP-nanodiscs at pH 8 was red-shifted by about 10 nm, relative to PR:DDM (Fig. 5, Table 2). SDS-PAGE analysis of the purified PR and GR MSP-nanodisc complexes would agree with the expected assembly ratio of two MSPDE31 molecules per incorporated protein unit (Fig. 5). DLS measurements indicate a hydrodynamic diameter of 14–15 nm for both the PR- and GR-MSP-nanodiscs (Table 2). Hence, all data support proper formation of pigment-incorporated nanodiscs for PR as well as GR. The pigments were extremely stable in the MSP-nanodisc environment and could be stored at 4 °C for at least several months without detectable loss of pigment.

To generate SMA-nanodiscs, the cellular membrane vesicles expressing the holo-protein were directly extracted with hydrolyzed SMA under high salt conditions at pH 8. The extraction required multiple rounds of sonication and incubation at RT for 5–7 days. About 60% of GR present in the *E. coli* membrane vesicles was extracted, in comparison to 30% extraction of PR. However, significant losses (20–30%) were incurred upon the subsequent purification steps, due to irreversible binding of these SMA-nanodisc complexes, which carry a high negative surface charge, to the Ni^{2+} column. Nonetheless, the nanodiscs could be isolated with a high degree of purity, as determined from the absorbance bands of the purified fractions, and SDS-PAGE analysis (Fig. 5). The absorbance bands of both PR- and GR:SMA-nanodiscs are significantly redshifted, as compared to the absorbance of the pigments in DDM (Table 2). Also in contrast to the MSP-nanodiscs, the SMA-nanodiscs were not very stable at 4 °C and even showed considerable loss of pigment after a month storage at −80 °C.

3.4. Photocycle of GR pigments embedded in DDM micelles or MSP-nanodisc complexes

In contrast to PR, the trimeric assembly of GR in MSP nanodiscs most likely is physiologically relevant, as discussed below, and is significantly more thermally stable than in a detergent environment, even when compared to DDM. Hence, the MSP micro-environment is a proper substitute for the native membrane, which presents an opportunity to identify any perturbation of the photocyle of GR by the DDM environment. The photodynamics of the native GR pigment (GR:A1) was investigated in DDM micelles and MSP-nanodiscs using transient absorption spectroscopy in the femto to submillisecond time range. The transient spectra were subjected to global analysis and fitted with eight time components. The corresponding evolution-associated difference spectra (EADS) and decay associated difference spectra (DADS) are

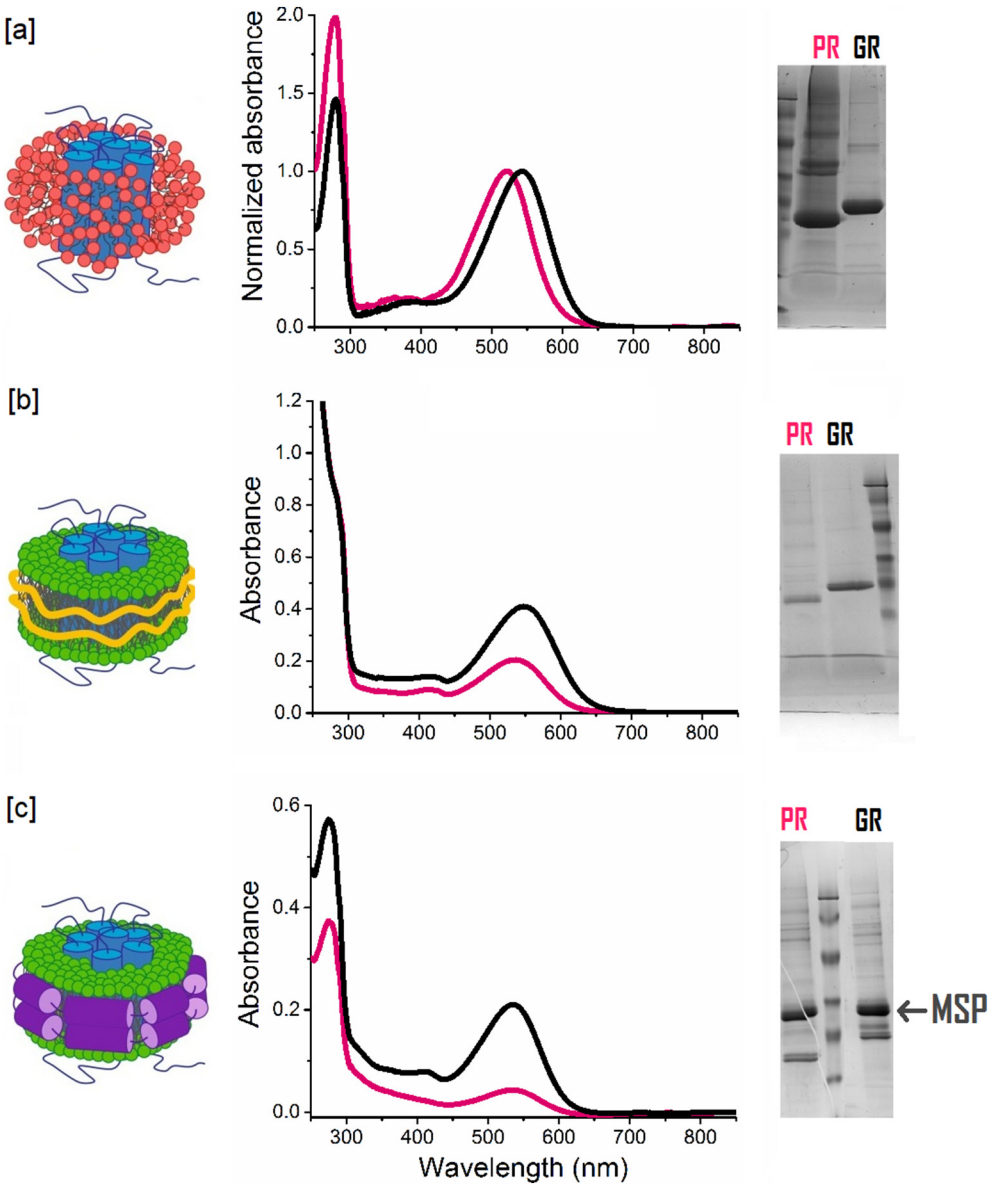

Fig. 5. Comparison between the different membrane-mimetic environments for 'solubilization' of PR (pink curves) and GR (black curves) in [a] DDM micelles, [b] SMA nanodiscs, or [c] MSP nanodiscs. Left panel: a schematic illustration of the environment with detergent molecules in red, lipids in green, SMA in yellow and MSP in purple, adapted from [71]. The middle panel shows absorbance spectra of the purified pigment-detergent/nanodisc complexes of PR (pink) and GR (black). Right panel: SDS-PAGE images of the purified fractions of PR (pink) and GR (black). The monomeric PR and GR bands migrate at ~22 kDa and ~25 kDa [a,b,c]. The main MSPDE31 band migrates at ~30 kDa, with the weaker lower band representing a truncated form of MSP.

Table 2
Comparison of purified pigment-detergent- and nanodisc complexes.

Environment	Pigment	λ_{max} (nm)[a]	d (nm)[b]	Yield (%)[c]
DDM	PR	520	nd	> 90
	GR	540	nd	> 95
MSP-nanodisc	PR	531	15	10
	GR	538	14	95
SMA-nanodisc	PR	537	28	20
	GR	548	21	40

[a] λ_{max} determined from the absorbance bands of the respective rhodopsin at pH 8; accuracy ± 2 nm.
[b] Average diameter of the nanodiscs determined by DLS; accuracy ± 1 nm.
[c] % yield or recovery of pigment in-nanodisc complexes after purification; accuracy ± 10%, nd = not determined.

shown in the Supporting Information (Fig. S1), and the time traces are displayed in Fig. 6. The rapid transitions up to ca 50 ps include excited-state decay and photoisomerization [36], i.e. formation of the first photoproduct (a K-like intermediate; absorbance band around 600 nm). In the time slot from femto- to picoseconds, the kinetics and corresponding spectral profiles are very similar in the DDM and nanodisc environment (Fig. S1). However, a significant difference was detected in the time constants of formation of the M–like photointermediate (absorbance band around 420 nm): 12 µs in DDM and 6.1 µs in nanodiscs (Figs. 6 and 7). Formation of the M-like photointermediate corresponds to the deprotonation of the retinal Schiff-base and initiates the proton transfer processes [36].

Previously, excited state decay time constants of 0.77 and 7.4 ps were reported for GR:A1 in DDM micelles, using bi-exponentially fitting at 955 nm [37]. The time constants we deduce here from a global fitting were ~2-fold shorter (Fig. S1). This is probably due to the different fitting procedures: we applied global fitting taking a spectral region of 380–670 nm into account, and probing ground-state bleach, excited-state absorption and product state absorption, while Iyer et al. applied bi-exponential fitting at a single wavelength at 955 nm, by probing stimulated emission.

Since the nanodisc environment seems to better preserve the slow phase of the photocycle, we turned to the 3-methoxyretinal A2 analog of GR (GR:MOA2). Previously we reported that the MOA2 analog pigments of PR and GR show large red-shifts in their absorbance maximum relative to the A1 pigments (65 and 80 nm, respectively; c.f. Fig. 8) [22]. However, both analog pigments only exhibit low proton pumping

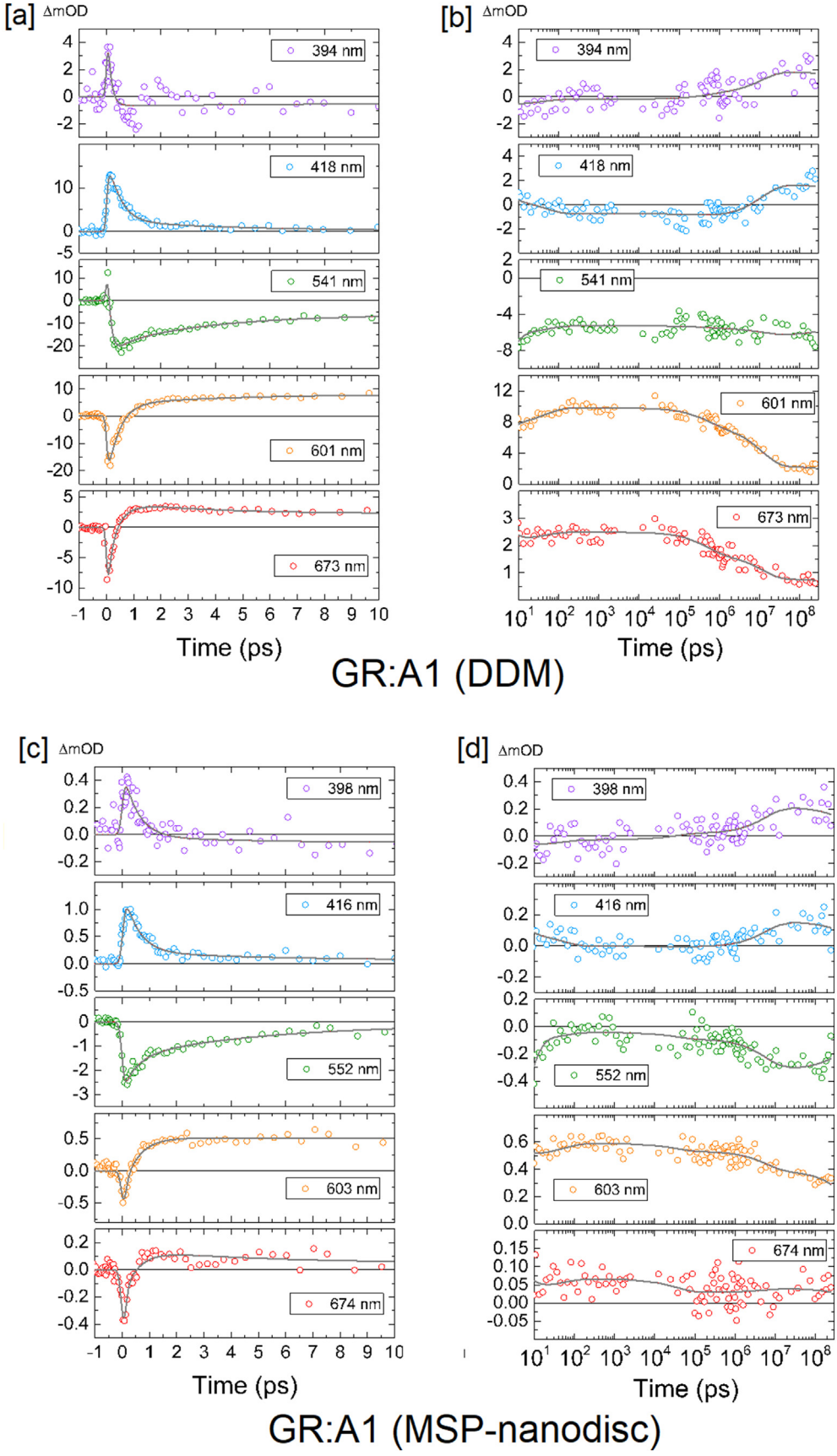

Fig. 6. Transient absorption data of GR:A1 extracted with global analysis. Selected time traces of GR:A1 in DDM micelles upon 570 nm excitation between [a] -1 to 10 ps and [b] 10 ps to 400 μs. Selected time traces of GR:A1 in MSP- nanodiscs upon 520 nm excitation between [c] -1 to 10 ps and [d] 10 ps to 400 μs. Open dots show the raw data and solid lines represent the fitted curves.

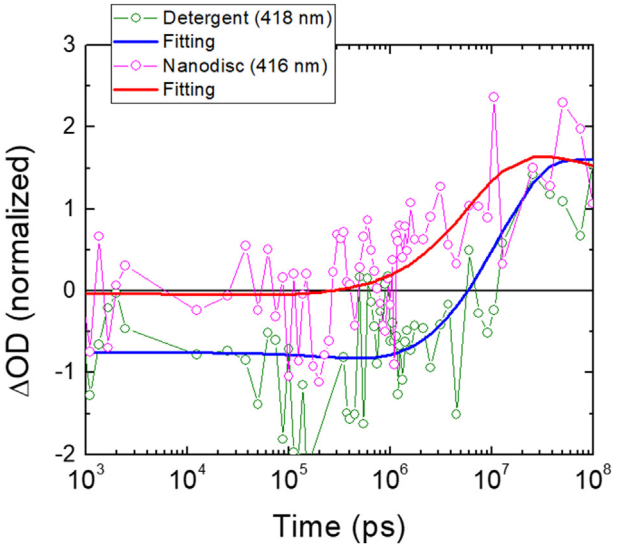

Fig. 7. Comparison of the kinetics of formation of the M-like photointermediate of GR:A1 in a DDM (blue-green) and in a lipid nanodisc (red) environment. Open dots show the raw data and solid lines represent the fitted curves.

activity under broadband white light illumination, and hardly any activity under narrow-band LED illumination [22]. Actually, upon analysis of PR:MOA2 by transient absorption spectroscopy in DDM micelles photoproduct formation was not detectable, and the excited states rapidly decayed to the ground state [38]. Since GR:MOA2 shows a bilobal CD spectrum in DDM as well as in nanodiscs, reflecting the trimeric organization (Fig. 6), we investigated whether photo-activation of GR:MOA2 would generate a photocycle in a DDM and/or a nanodisc environment. The photodynamics of GR:MOA2 in DDM are very similar to those of PR:MOA2 in DDM [38], with no detectable photoproducts and relaxation to the ground state with a time constant of 4.6 ps (Figs. S2, S3). As a matter of fact, the data we extracted from the photodynamics of GR:MOA2 in nanodiscs are almost identical to those of the DDM sample (Figs. S2, S3), with rapid decay of the excited states to the initial ground state (5.0 ps time constant) and no indication for photoproduct formation.

4. Discussion

4.1. Differences between the detergent systems investigated

A wide variety of detergents exist with different combinations of head and tail groups [1] and the size of protein-detergent micellar complexes usually depends on the polar head of the detergent. However, the detergent shell usually is not able to sustain the structural stability and functional activity of membrane proteins to the same extent as the native lipid micro-environment [2,3]. Hence, it is a challenge to select a suitable detergent to properly solubilize and stabilize a

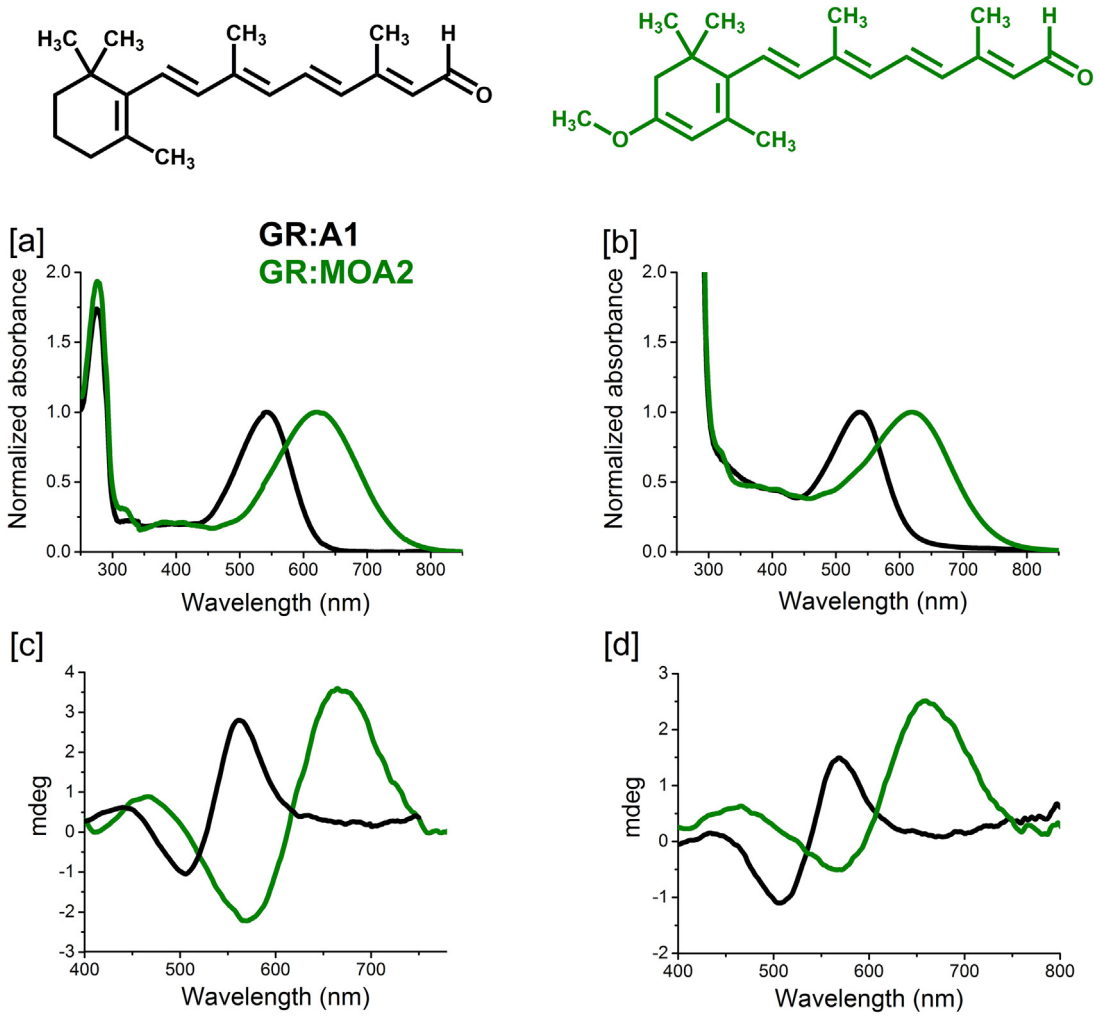

Fig. 8. Top panel: Absorbance spectra of GR:A1 (black curve) and GR:MOA2 (green curve) purified in 2% DDM [a] or in MSP-nanodisc complexes [b] at pH 8. Bottom panel: circular dichroism spectra of the above in 2% DDM [c] or MSP-nanodiscs [d].

particular membrane protein, both because of the poorly defined properties of pigment-detergent complexes and because of the individual demands of a protein. Our results clearly support the consensus that the choice of surfactant may have a significant effect on the oligomeric organization and corresponding stability of membrane proteins. The nonionic sugar-based detergent DDM [4] has been extensively used in membrane protein studies. DDM forms large, well-structured micelles (Table 1; 56–71 kDa) with a relatively large lateral pressure, thereby stabilizing protein dynamics and protein-protein contacts quite well, and minimizing denaturation [1]. Previous studies have shown that the native oligomeric assembly of PR and GR is preserved in DDM micelles. PR contains a predominant fraction of penta- and hexamers and a minor monomeric population, while GR is mainly organized as a trimer [29–32,39,40] which agrees with our analyses (Fig. 4), although very recently also a pentameric assembly of GR has been reported [41]. A native oligomeric state will contribute to the relatively high thermal stability of PR and GR in DDM micelles. However, the large protein-detergent complexes formed by DDM make it less suitable as a detergent of choice for crystallization trials, and for structural studies using solution-state NMR. Smaller protein-detergent complexes, which would stabilize a solubilized monomer are highly desirable. Here, we have compared a number of commonly used detergent environments, and their influence on the thermal stability, oligomeric structure and spectral properties of PR and GR as representatives of a proton-pump family of membrane proteins.

A variant of the zwitterionic detergent DPC was recently used to solve the solution NMR structure of PR [40]. DPC forms much smaller micelles than DDM (Table 1; 18–21 kDa) and is hence more useful to isolate the monomeric form of these proteins [31]. However, in our study, DPC was found to be the most destabilizing of all detergents tested, which would agree with a recent review on DPC effects on membrane protein structure [42]. Despite rapid solubilization and purification steps carried out in the cold, extensive denaturation was observed, in particular for GR, accompanied by release of retinal (Fig. 3). We thereby decided to focus on nonionic detergents such as TritonX-100, OG and OGNG, of which OG also forms smaller protein-detergent complexes. Prior studies have shown that solubilization of PR with 13% TritonX-100 stabilizes a monomeric red-shifted fraction of PR [43]. However, we found that though the solubilization efficiency of TritonX-100 was high, at concentrations higher than 10% it did not stabilize the pigments sufficiently for long-term storage or further characterization. OG showed good solubilization efficiency, however at the concentration required to increase the monomer population ($> 2\%$) the pigments showed poor thermal stability upon storage at 4 °C. Despite its poor solubilization potential, OGNG came out as the most stabilizing detergent of this triad, with no significant loss of intact pigment, even upon incubation at RT for several days. We thereby decided to investigate the oligomeric distribution of PR and GR in OGNG using SEC and CD, so as to compare it to the well-characterized DDM microenvironment. From the SEC distribution, we conclude that in OGNG micelles, both PR and GR most likely largely exist in monomeric form.

The CD spectra of PR and GR in DDM exhibit a strong bilobal bandshape (Fig. 4c), centered around the absorption maxima of the pigments. Such a bandshape was also observed in the CD spectrum of other microbial rhodopsins [34,35,44–48], and was also reported for trimeric GR in DDM [29,30] and for GR in the *E. coli* membrane [30]. It is thought to originate from an oligomeric complex of the pigment due to excitonic interactions between the retinal molecules [35]. Hence, such a strong bilobal bandshape is not expected for monomeric units of these pigments. Indeed, the CD spectra of the pigments purified in OGNG (Fig. 4d) show a strong reduction in intensity and loss of bilobal structure, which would agree with a predominant monomeric state [29,30]. This finding supports the SEC data and we conclude that the OGNG micelles mainly contain PR or GR monomers.

In OGNG micelles, and to a smaller extent in OG micelles, a significant red-shift in the absorbance bands of both PR and GR was observed relative to DDM micelles (11–13 nm; Table 1). Saccharide headgroups (i.e. present in DDM, OG and OGNG) are likely to have a minimal effect on the retinal-protein interaction [5]. A red-shift was also reported for PR in DHPC micelles [49]. Besides, such a red-shift is also observed for PR in SMA- as well as in MSP-nanodiscs, and for GR in SMA-nanodiscs (Table 2). It is likely that the oligomeric state of PR and GR plays an important role in this shift. It was shown that in the hexameric and pentameric complexes of PR, the pKa of D97 (6.5–6.7) is about one unit lower than in monomeric PR (7.4–7.8) [31,32]. Presumably this originates in the cross-protomer interaction between H75-W34, which reduces the weakening effect of H75 on the acidity of D97 [22]. The absence of this H75-W34 interaction in the monomer thus enhances protonation of D97 in the pH range 6–9, thereby inducing a red-shift. This is further evidence for a monomeric state of PR in OGNG micelles. The red-shift in the absorbance band of GR (Table 1), however, is not easily explained, since the equivalent counterion D121 in GR has a lower pKa (≈ 4.8) and GR's absorbance band shows little pH dependence in the range 6–9 [31]. Possibly, the His87-Asp121 interaction is modified in the GR monomer, which can affect the pKa of the counterion [31]. In fact, in thermophilic rhodopsin, which is trimeric in DDM micelles, transition from the trimeric to a stable monomeric organization is accompanied by a 6 nm blueshift in the absorbance band [50]. The same treatment of GR results in a 9 nm redshift [50]. This further supports our interpretation for the GR state in OGNG micelles.

4.2. MSP and SMA pigment-nanodisc complexes

Protein-containing MSP-nanodiscs are discoid monodisperse open complexes, which consist of the protein of interest, embedded in a phospholipid bilayer, enclosed by two amphipathic MSP molecules. The complex is “open” since it is accessible to all solutes from both sides (Figs. 1, 5). These nanodiscs are usually 9–20 nm wide, with the diameter of the nanodisc being controlled by the length of the MSP used [7]. Instead, SMA nanodiscs are enclosed by a short styrene-maleic acid copolymer [14]. The advantage of SMA-nanodiscs is that they do not require prior solubilization of the protein by detergents. The small size of both nanodisc systems leads to optical near-transparency of a sample, due to which nanodiscs have been widely used in a variety of spectroscopic techniques.

We generated both types, i.e. MSP and SMA-nanodiscs. Generation of SMA-nanodiscs required longer incubation steps, and we noticed that the rhodopsin-SMA nanodiscs complexes had poor thermal stability, despite the native-like membrane environment. The multiple sonication steps could have had an impact on the structure of the resulting complexes, in combination with the high ionic strength (0.5 M NaCl) required to partially neutralize the negative surface charge on the SMA copolymer. We further observed that, in general, GR was more readily incorporated into the nanodisc environment than PR. This is attributed to the oligomeric assembly of the pigments in the native membrane.

Various studies have shown that PR exists predominantly as hexamers or pentamers both in DDM [51] and in the membrane environment, via crystallography of the close relative blue absorbing PR [52,53], pulsed EPR [33,39], mass spectrometry [54], solid-state NMR [55] and atomic force microscopy in lipid bilayers [45,51,56]. Cross-linking studies have further shown that hexamers of PR can be found in the native *E. coli* membrane, indicating that this assembly is most likely physiological [31]. A previous study showed that PR was reconstituted into MSP-nanodiscs as photoactive monomers after solubilization in high concentrations of TritonX-100 [43]. Considering the diameter of the MSP-nanodiscs, we generated, (14–15 nm) and that of the oligomeric PR complexes (ca 10 nm) [31,45], we conclude that the predominantly hexameric population of PR is too large to be comfortably contained within a MSP-nanodisc. Thus, we primarily isolate nanodiscs containing the smaller monomeric fraction of PR, which explains the much lower yield of PR nanodiscs, as compared to GR nanodiscs. This is

further corroborated by the red-shifted absorbance bands of the purified PR-nanodiscs relative to DDM micelles due to the higher pKa of D97 in the monomers. On the other hand, GR is thought to mainly exist as a trimer in DDM in the pH range 6–9 [29,30,57], which agrees with our data (Fig. 4), but is in conflict with recent studies that report pentamers in membranes based upon flat nanodisc preparations [45] and an EPR-DEER analysis based on the GR crystal structure [41]. In view of the easily perturbed equilibrium between the GR protomers [30], we consider it most likely that the GR-trimer represents one of its possible physiological forms in the membrane. Accordingly, trimers of GR would easily incorporate within MSP-nanodiscs, since trimeric bR and LHCII, proteins of similar size, are well contained in such nanodiscs [20,58].

The striking observation of a significant red-shift of PR (17 nm) and GR (8 nm) after incorporation into SMA-nanodiscs (Table 2) is still unexplained. The measured size of these nanodiscs (Table 2, a diameter of 28 and 21 nm, for PR and GR respectively), suggests that they could easily contain GR as well as PR in their physiological oligomeric state. The yield of SMA-nanodiscs was too low for analysis with CD spectroscopy. The low local pH at the surface of the highly charged SMA nanodiscs may contribute towards this redshift. Furthermore, the harsh conditions required to generate the SMA-nanodiscs may have led towards conformational deformation, affecting protein structure as well as protein-ligand and protomer-protomer interaction. This is likely to have an impact on the photodynamics of the pigment, as recently reported for sensory rhodopsin II [59]. Possibly, supplementation with extra lipid during protein extraction could alleviate these conditions, as recently reported for some G protein-coupled receptors [60].

4.3. Transient absorption spectroscopy of GR in a DDM or nanodisc environment

Due to the high thermal stability of MSP-nanodiscs, and the ease of incorporation of a physiologically relevant assembly of GR, we decided to compare GR photodynamics in GR:MSP-nanodiscs as a biomimetic system with GR in DDM micelles. Using ultrafast pump-probe spectroscopy, we could observe the early photointermediates in the photocycle of GR:A1 up until the formation of the M-intermediate, which corresponds to the deprotonation of the Schiff-base. Overall, the femto- and picosecond components are comparable across the detergent and the lipid-nanodisc environment with respect to both the spectral properties and dynamics (Fig. S1), showing a minimal impact of the detergent environment on photoisomerization. This is not surprising, since in this time range the protein structure only allows minor conformational changes, which are largely confined to the binding site [61]. However, the formation of the M-like photointermediate is about 2-fold faster in the lipid nanodisc environment, as compared to the DDM micelles. This is in agreement with previous studies which have reported a faster turnover for PR:A1 in both proteoliposomes and the nanodiscs [49,62], with an ~2.5 fold acceleration of M-like photointermediate formation in nanodisc as compared to DDM micelles [49]. It is reported that in DDM micelles membrane proteins have a larger conformational space than in a lipid bilayer [1,9], which may slow down vectorial processes like the proton transfer accompanying M-state formation. A slower M-formation for PR has also been reported in a more aggressive TritonX-100 surfactant environment [32]. These data support the concept that while a mild detergent environment preserves the ultra-fast dynamics of membrane proteins, investigation of the slower dynamics involving conformational changes and ion transfer or substrate binding could benefit from incorporation of the pigment in a proper bilayer environment, which is well represented by MSP-nanodiscs [7,20,43,58,63,64]. The size of MSP-nanodiscs is small, which precludes incorporation of larger oligomeric units like pentamers and hexamers of PR and membrane-bound signalosome complexes. However, novel developments like the more flexible saposin or DNA scaffolds can significantly expand the range of accessible nanodisc dimensions, and open up this field also for large membrane protein complexes [65–67].

We did not detect evidence for a photocycle upon excitation of GR:MOA2, whether in DDM micelles or in MSP-nanodiscs. (Fig. 7). Apparently, a lipid environment cannot sustain a photocycle in the GR:MOA2 pigment either. This would account for our earlier observations that in the *E. coli* cell membrane PR:MOA2 and GR:MOA2 pigments do not show proton pump activity upon excitation with narrow-band LED light [22]. The electronegative character of the methoxy group in MOA2, partially responsible for the large bathochromic shift of the absorbance band (Fig. 6), may also contribute to this serious loss in activity. A theoretical study indicates that substituents in the chromophore perturbing the conjugated π-electron system may also strongly affect the photoisomerization mechanism and kinetics [68].

5. Conclusion

The selection of a proper biomimetic system is crucial for structural and functional studies of membrane proteins. We therefore tested various detergents and nanodisc complexes to assess their effect on the spectral properties, thermal stability, structural state and photodynamics of PR and/or GR. Overall, the least deleterious effects of the detergents tested were observed for DDM and OGNG. For solution NMR and crystallographic studies of PR and GR, OGNG would be an interesting option, since it maintains good thermal stability of the monomer of both rhodopsins. For spectroscopic studies in a native-like state we recommend a MSP-nanodisc-bilayer environment for GR, since this combination is thermally very stable, produces little light-scattering thanks to its small size, and substitutes for the natural membrane environment quite well. The DDM micelle is a good option for penta- and hexameric PR, since it combines good thermal stability with medium-sized micelles. With the newer bilayer scaffold systems (like saposin, DNA) incorporation of hexameric PR in a nanodisc bilayer should be feasible, but this will be at the expense of higher light scattering levels. For biophysical studies of the monomeric rhodopsins, again OGNG would be most appropriate. In general, as also indicated by other studies [3,7,12,20,43,49,58,63,64,69] the nanodisc-bilayer environment is recommended for characterizing the photocycle and functional dynamics of rhodopsins as a substitute for the natural membrane environment, with MSP-nanodiscs having the advantage of low light scattering.

Transparency document

The Transparency document associated with this article can be found, in online version.

Acknowledgements

We would like to thank Hans Den Dulk, Nora Goosen and Gerry Moolenaar for their technical advice and support.

Funding

This study was financially supported by the BioSolar Cell consortium and Leiden University. The project was carried out in the research programme of BioSolar Cells (BSC core project grant C2.9 to W.J.d.G and K.J.H), co-financed by the Dutch Ministry of Economic Affairs. Y.H. and J.T.M.K. were supported by the Chemical Sciences Council of the Netherlands Organisation for Scientific Research (NWO-CW) through a VICI grant to J.T.M.K.

Appendix A. Supplementary data

Supplementary data to this article can be found online at https://doi.org/10.1016/j.bbamem.2019.183113.

References

[1] A. Sadaf, K.H. Cho, B. Byrne, P.S. Chae, Amphipathic agents for membrane protein study, Methods Enzymol. 557 (2015) 57–94.
[2] A.M. Seddon, P. Curnow, P.J. Booth, Membrane proteins, lipids and detergents: not just a soap opera, Biochim. Biophys. Acta 1666 (1–2) (2004) 105–117.
[3] H.X. Zhou, T.A. Cross, Influences of membrane mimetic environments on membrane protein structures, Annu. Rev. Biophys. 42 (2013) 361–392.
[4] W.J. De Grip, P.H.M. Bovee-Geurts, Synthesis and properties of alkylglucosides with mild detergent action: improved synthesis and purification of β-1-octyl-, -nonyl-, and -decyl-glucose. Synthesis of β-1-undecylglucose and β-1-dodecylmaltose, Chem. Phys. Lipids 23 (4) (1979) 321–335.
[5] W.J. De Grip, Thermal stability of rhodopsin and opsin in some novel detergents, Meth Enzymol. (1982) 256–265.
[6] D.C. Mitchell, Progress in understanding the role of lipids in membrane protein folding, Biochim. Biophys. Acta Biomembr. 1818 (4) (2012) 951–956.
[7] I.G. Denisov, S.G. Sligar, Nanodiscs in membrane biochemistry and biophysics, Chem. Rev. 117 (6) (2017) 4669–4713.
[8] S.J. Opella, Solid-state NMR and membrane proteins, J. Magn. Reson. 253 (2015) 129–137.
[9] J.L. Popot, T. Althoff, D. Bagnard, J.L. Banères, P. Bazzacco, E. Billon-Denis, L.J. Catoire, P. Champeil, D. Charvolin, M.J. Cocco, G. Crémel, T. Dahmane, L.M. de la Maza, C. Ebel, F. Gabel, F. Giusti, Y. Gohon, E. Goormaghtigh, E. Guittet, J.H. Kleinschmidt, W. Kühlbrandt, C. Le Bon, K.L. Martinez, M. Picard, B. Pucci, J.N. Sachs, C. Tribet, C. van Heijenoort, F. Wien, F. Zito, M. Zoonens, Amphipols from A to Z, Annu. Rev. Biophys. 40 (1) (2011) 379–408.
[10] T. Friedrich, S. Geibel, R. Kalmbach, I. Chizhov, K. Ataka, J. Heberle, M. Engelhard, E. Bamberg, Proteorhodopsin is a light-driven proton pump with variable vectoriality, J. Mol. Biol. 321 (5) (2002) 821–838.
[11] T.H. Bayburt, S.G. Sligar, Membrane protein assembly into nanodiscs, FEBS Lett. 584 (9) (2010) 1721–1727.
[12] N. Shirzad-Wasei, J. van Oostrum, P.H. Bovee-Geurts, L.J. Kusters, G.J. Bosman, W.J. DeGrip, Rapid transfer of overexpressed integral membrane protein from the host membrane into soluble lipid nanodiscs without previous purification, Biol. Chem. 396 (8) (2015) 903–915.
[13] Y. Cai, Y. Liu, K.J. Culhane, B.T. DeVree, Y. Yang, R.K. Sunahara, E.C.Y. Yan, Purification of family B G protein-coupled receptors using nanodiscs: application to human glucagon-like peptide-1 receptor, PLoS One 12 (6) (2017) e0179568.
[14] J.M. Dörr, M.C. Koorengevel, M. Schafer, A.V. Prokofyev, S. Scheidelaar, E.A. van der Cruijsen, T.R. Dafforn, M. Baldus, J.A. Killian, Detergent-free isolation, characterization, and functional reconstitution of a tetrameric K+ channel: the power of native nanodiscs, Proc. Natl. Acad. Sci. U. S. A. 111 (52) (2014) 18607–18612.
[15] O. Béjà, L. Aravind, E.V. Koonin, M.T. Suzuki, A. Hadd, L.P. Nguyen, S.B. Jovanovich, C.M. Gates, R.A. Feldman, J.L. Spudich, E.N. Spudich, E.F. DeLong, Bacterial rhodopsin: evidence for a new type of phototrophy in the sea, Science 289 (5486) (2000) 1902–1906.
[16] Y. Nakamura, T. Kaneko, S. Sato, M. Mimuro, H. Miyashita, T. Tsuchiya, S. Sasamoti, A. Watanabe, K. Kawashima, Y. Kishida, C. Kiyokawa, M. Kohara, M. Matsumoto, A. Matsuno, N. Nakazaki, S. Simpo, C. Takeuchi, M. Yamada, S. Tabata, Complete genome structure of Gloeobacter violaceus PCC7421, a cyanobacterium that lacks thylakoids. *DNA Res* 10 (2003) 137–145.
[17] C. Bamann, E. Bamberg, J. Wachtveitl, C. Glaubitz, Proteorhodopsin, Biochim. Biophys. Acta 1837 (5) (2014) 614–625.
[18] W.J. De Grip, J. Van Oostrum, P.H.M. Bovee-Geurts, Selective detergent-extraction from mixed detergent/lipid/protein micelles, using cyclodextrin inclusion compounds: a novel generic approach for the preparation of proteoliposomes, Biochem. J. 330 (Pt 2) (1998) 667–674.
[19] S.Y. Kim, S.A. Waschuk, L.S. Brown, K.H. Jung, Screening and characterization of proteorhodopsin color-tuning mutations in Escherichia coli with endogenous retinal synthesis, Biochim. Biophys. Acta 1777 (6) (2008) 504–513.
[20] A. Pandit, N. Shirzad-Wasei, L.M. Wlodarczyk, H. van Roon, E.J. Boekema, J.P. Dekker, W.J. de Grip, Assembly of the major light-harvesting complex II in lipid nanodiscs, Biophys. J. 101 (10) (2011) 2507–2515.
[21] S. Ganapathy, O. Bécheau, H. Venselaar, S. Frölich, J.B. van der Steen, Q. Chen, S. Radwan, J. Lugtenburg, K.J. Hellingwerf, H.J. de Groot, W.J. de Grip, Modulation of spectral properties and pump activity of proteorhodopsins by retinal analogues, Biochem. J. 467 (2) (2015) 333–343.
[22] S. Ganapathy, H. Venselaar, Q. Chen, H.J.M. de Groot, K.J. Hellingwerf, W.J. de Grip, Retinal-based proton pumping in the near infrared, J. Am. Chem. Soc. 139 (6) (2017) 2338–2344.
[23] Y. Hontani, S. Ganapathy, S. Frehan, M. Kloz, W.J. de Grip, J.T.M. Kennis, Strong pH-dependent near-infrared fluorescence in a microbial rhodopsin reconstituted with a red-shifting retinal analogue, J. Phys. Chem. Lett. 9 (22) (2018) 6469–6474.
[24] J. Ravensbergen, F.F. Abdi, J.H. van Santen, R.N. Frese, B. Dam, R. van de Krol, J.T.M. Kennis, Unraveling the carrier dynamics of $BiVO_4$: a femtosecond to microsecond transient absorption study, J. Phys. Chem. C 118 (48) (2014) 27793–27800.
[25] Y. Hontani, M. Marazzi, K. Stehfest, T. Mathes, I.H.M. van Stokkum, M. Elstner, P. Hegemann, J.T.M. Kennis, Reaction dynamics of the chimeric channelrhodopsin C1C2, Sci. Rep. 7 (1) (2017) 7217.
[26] J.J. Snellenburg, S. Laptenok, R. Seger, K.M. Mullen, I.H.M. van Stokkum, Glotaran: a Java-based graphical user interface for the R package TIMP, J. Stat. Softw. 49 (3) (2012) 1–22.
[27] P.S. Chae, R.R. Rana, K. Gotfryd, S.G.F. Rasmussen, A.C. Kruse, K.H. Cho, S. Capaldi, E. Carlsson, B. Kobilka, C.J. Loland, U. Gether, S. Banerjee, B. Byrne, J.K. Lee, S.H. Gellman, Glucose-neopentyl glycol (GNG) amphiphiles for membrane protein study, Chem. Commun. 49 (23) (2013) 2287–2289.
[28] D.E. Warschawski, A.A. Arnold, M. Beaugrand, A. Gravel, É. Chartrand, I. Marcotte, Choosing membrane mimetics for NMR structural studies of transmembrane proteins, Biochim. Biophys. Acta Biomembr. 1808 (8) (2011) 1957–1974.
[29] A. Iizuka, K. Kajimoto, T. Fujisawa, T. Tsukamoto, T. Aizawa, N. Kamo, K.-H. Jung, M. Unno, M. Demura, T. Kikukawa, Functional importance of the oligomer formation of the cyanobacterial H^+ pump Gloeobacter rhodopsin, Sci. Rep. 9 (1) (2019) 10711.
[30] T. Tsukamoto, T. Kikukawa, T. Kurata, K.H. Jung, N. Kamo, M. Demura, Salt bridge in the conserved His-Asp cluster in Gloeobacter rhodopsin contributes to trimer formation, FEBS Lett. 587 (4) (2013) 322–327.
[31] S. Hussain, M. Kinnebrew, N.S. Schonenbach, E. Aye, S. Han, Functional consequences of the oligomeric assembly of proteorhodopsin, J. Mol. Biol. 427 (6 Pt B) (2015) 1278–1290.
[32] M.N. Idso, N.R. Baxter, S. Narayanan, E. Chang, J. Fisher, B.F. Chmelka, S. Han, Proteorhodopsin function is primarily mediated by oligomerization in different micellar surfactant solutions, J. Phys. Chem. B 123 (19) (2019) 4180–4192.
[33] D.T. Edwards, T. Huber, S. Hussain, K.M. Stone, M. Kinnebrew, I. Kaminker, E. Matalon, M.S. Sherwin, D. Goldfarb, S. Han, Determining the oligomeric structure of proteorhodopsin by Gd^{3+}-based pulsed dipolar spectroscopy of multiple distances, Structure 22 (11) (2014) 1677–1686.
[34] H. Vogel, W. Gartner, The secondary structure of bacteriorhodopsin determined by Raman and circular dichroism spectroscopy, J. Biol. Chem. 262 (24) (1987) 11464–11469.
[35] J.Y. Cassim, Unique biphasic band shape of the visible circular dichroism of bacteriorhodopsin in purple membrane: Excitons, multiple transitions or protein heterogeneity? Biophys. J. 63 (5) (1992) 1432–1442.
[36] O.P. Ernst, D.T. Lodowski, M. Elstner, P. Hegemann, L.S. Brown, H. Kandori, Microbial and animal rhodopsins: structures, functions, and molecular mechanisms, Chem. Rev. 114 (1) (2014) 126–163.
[37] E.S.S. Iyer, R. Misra, A. Maity, O. Liubashevski, Y. Sudo, M. Sheves, S. Ruhman, Temperature independence of ultrafast photoisomerization in thermophilic rhodopsin: assessment versus other microbial proton pumps, J. Am. Chem. Soc. 138 (38) (2016) 12401–12407.
[38] Y. Hontani, S. Ganapathy, S. Frehan, M. Kloz, W.J. de Grip, J.T.M. Kennis, Photoreaction dynamics of red-shifting retinal analogues reconstituted in proteorhodopsin, J. Phys. Chem. B 123 (19) (2019) 4242–4250.
[39] K.M. Stone, J. Voska, M. Kinnebrew, A. Pavlova, M.J. Junk, S. Han, Structural insight into proteorhodopsin oligomers, Biophys. J. 104 (2) (2013) 472–481.
[40] S. Reckel, D. Gottstein, J. Stehle, F. Lohr, M.K. Verhoefen, M. Takeda, R. Silvers, M. Kainosho, C. Glaubitz, J. Wachtveitl, F. Bernhard, H. Schwalbe, P. Guntert, V. Dotsch, Solution NMR structure of proteorhodopsin, Angew Chem Int Ed Engl 50 (50) (2011) 11942–11946.
[41] T. Morizumi, W.-L. Ou, N. Van Eps, K. Inoue, H. Kandori, L.S. Brown, O.P. Ernst, X-ray crystallographic structure and oligomerization of Gloeobacter rhodopsin, Sci. Rep. 9 (1) (2019) 11283.
[42] C. Chipot, F. Dehez, J.R. Schnell, N. Zitzmann, E. Pebay-Peyroula, L.J. Catoire, B. Miroux, E.R.S. Kunji, G. Veglia, T.A. Cross, P. Schanda, Perturbations of native membrane protein structure in alkyl phosphocholine detergents: a critical assessment of NMR and biophysical studies, Chem. Rev. 118 (7) (2018) 3559–3607.
[43] M.J. Ranaghan, C.T. Schwall, N.N. Alder, R.R. Birge, Green proteorhodopsin reconstituted into nanoscale phospholipid bilayers (nanodiscs) as photoactive monomers, J. Am. Chem. Soc. 133 (45) (2011) 18318–18327.
[44] E. Smolensky, M. Sheves, Retinal-salinixanthin interactions in xanthorhodopsin: a circular dichroism (CD) spectroscopy study with artificial pigments, Biochemistry 48 (34) (2009) 8179–8188.
[45] M. Shibata, K. Inoue, K. Ikeda, M. Konno, M. Singh, C. Kataoka, R. Abe-Yoshizumi, H. Kandori, T. Uchihashi, Oligomeric states of microbial rhodopsins determined by high-speed atomic force microscopy and circular dichroic spectroscopy, Sci. Rep. 8 (1) (2018) 8262.
[46] C.A. Hasselbacher, J.L. Spudich, T.G. Dewey, Circular dichroism of halorhodopsin: comparison with bacteriorhodopsin and sensory rhodopsin I, Biochemistry 27 (7) (1988) 2540–2546.
[47] T. Sasaki, M. Kubo, T. Kikukawa, M. Kamiya, T. Aizawa, K. Kawano, N. Kamo, M. Demura, Halorhodopsin from natronomonas pharaonis forms a trimer even in the presence of a detergent, dodecyl-β-d-maltoside, Photochem. Photobiol. 85 (1) (2009) 130–136.
[48] R. Misra, A. Hirshfeld, M. Sheves, Molecular mechanism for thermal denaturation of thermophilic rhodopsin, Chem. Sci. 10 (31) (2019) 7365–7374.
[49] K. Mors, C. Roos, F. Scholz, J. Wachtveitl, V. Dotsch, F. Bernhard, C. Glaubitz, Modified lipid and protein dynamics in nanodiscs, Biochim. Biophys. Acta 1828 (4) (2013) 1222–1229.
[50] T. Tsukamoto, M. Demura, Y. Sudo, Irreversible trimer to monomer transition of thermophilic rhodopsin upon thermal stimulation, J. Phys. Chem. B 118 (43) (2014) 12383–12394.
[51] A.L. Klyszejko, S. Shastri, S.A. Mari, H. Grubmuller, D.J. Muller, C. Glaubitz, Folding and assembly of proteorhodopsin, J. Mol. Biol. 376 (1) (2008) 35–41.
[52] S. Shastri, J. Vonck, N. Pfleger, W. Haase, W. Kuehlbrandt, C. Glaubitz, Proteorhodopsin: characterisation of 2D crystals by electron microscopy and solid state NMR, Biochim. Biophys. Acta 1768 (12) (2007) 3012–3019.
[53] T. Ran, G. Ozorowski, Y. Gao, O.A. Sineshchekov, W. Wang, J.L. Spudich, H. Luecke, Cross-protomer interaction with the photoactive site in oligomeric proteorhodopsin complexes, Acta Crystallogr D Biol Crystallogr 69 (10) (2013) 1965–1980.
[54] J. Hoffmann, L. Aslimovska, C. Bamann, C. Glaubitz, E. Bamberg, B. Brutschy,

Studying the stoichiometries of membrane proteins by mass spectrometry: microbial rhodopsins and a potassium ion channel, Phys. Chem. Chem. Phys. 12 (14) (2010) 3480–3485.
[55] J. Maciejko, M. Mehler, J. Kaur, T. Lieblein, N. Morgner, O. Ouari, P. Tordo, J. Becker-Baldus, C. Glaubitz, Visualizing specific cross-protomer interactions in the homo-oligomeric membrane protein proteorhodopsin by dynamic-nuclear-polarization-enhanced solid-state NMR, J. Am. Chem. Soc. 137 (28) (2015) 9032–9043.
[56] H. Liang, G. Whited, C. Nguyen, G.D. Stucky, The directed cooperative assembly of proteorhodopsin into 2D and 3D polarized arrays, Proc. Natl. Acad. Sci. U. S. A. 104 (20) (2007) 8212–8217.
[57] Q. Chen, J. Arents, S. Ganapathy, W.J. de Grip, K.J. Hellingwerf, Functional expression of Gloeobacter rhodopsin in Synechocystis sp. PCC6803, Photochem Photobiol 93 (3) (2017) 772–781.
[58] T.H. Bayburt, Y.V. Grinkova, S.G. Sligar, Assembly of single bacteriorhodopsin trimers in bilayer nanodiscs, Arch. Biochem. Biophys. 450 (2) (2006) 215–222.
[59] Mosslehy, W., N. Voskoboynikova, A. Colbasevici, A. Ricke, D. Klose, J.P. Klare, A. Y. Mulkidjanian, and H.-J. Steinhoff, Conformational dynamics of sensory rhodopsin II in nanolipoprotein and styrene–maleic acid lipid particles. *Photochemistry and Photobiology*, 2019. **0**(0).
[60] J. Broecker, B.T. Eger, O.P. Ernst, Crystallogenesis of membrane proteins mediated by polymer-bounded lipid nanodiscs, Structure 25 (2) (2017) 384–392.
[61] P. Nogly, T. Weinert, D. James, S. Carbajo, D. Ozerov, A. Furrer, D. Gashi, V. Borin, P. Skopintsev, K. Jaeger, K. Nass, P. Båth, R. Bosman, J. Koglin, M. Seaberg, T. Lane, D. Kekilli, S. Brünle, T. Tanaka, W. Wu, C. Milne, T. White, A. Barty, U. Weierstall, V. Panneels, E. Nango, S. Iwata, M. Hunter, I. Schapiro, G. Schertler, R. Neutze, J. Standfuss, Retinal isomerization in bacteriorhodopsin captured by a femtosecond x-ray laser, Science 361 (6398) (2018) eaat0094.
[62] L. Lindholm, C. Arioz, M. Jawurek, J. Liebau, L. Maler, A. Wieslander, C. von Ballmoos, A. Barth, Effect of lipid bilayer properties on the photocycle of green proteorhodopsin, Biochim. Biophys. Acta 1847 (8) (2015) 698–708.
[63] C. Roos, M. Zocher, D. Müller, D. Münch, T. Schneider, H.-G. Sahl, F. Scholz, J. Wachtveitl, Y. Ma, D. Proverbio, E. Henrich, V. Dötsch, F. Bernhard, Characterization of co-translationally formed nanodisc complexes with small multidrug transporters, proteorhodopsin and with the E. coli MraY translocase, Biochim. Biophys. Acta Biomembr. 1818 (12) (2012) 3098–3106.
[64] I. Shimada, T. Ueda, Y. Kofuku, M.T. Eddy, K. Wüthrich, GPCR drug discovery: integrating solution NMR data with crystal and cryo-EM structures, Nat. Rev. Drug Discov. 18 (2018) 59.
[65] J. Frauenfeld, R. Löving, J.-P. Armache, A.F.P. Sonnen, F. Guettou, P. Moberg, L. Zhu, C. Jegerschöld, A. Flayhan, J.A.G. Briggs, H. Garoff, C. Löw, Y. Cheng, P. Nordlund, A saposin-lipoprotein nanoparticle system for membrane proteins, Nat. Methods 13 (2016) 345.
[66] C.-T.H. Chien, L.R. Helfinger, M.J. Bostock, A. Solt, Y.L. Tan, D. Nietlispach, An adaptable phospholipid membrane mimetic system for solution NMR studies of membrane proteins, J. Am. Chem. Soc. 139 (42) (2017) 14829–14832.
[67] K. Iric, M. Subramanian, J. Oertel, N.P. Agarwal, M. Matthies, X. Periole, T.P. Sakmar, T. Huber, K. Fahmy, T.L. Schmidt, DNA-encircled lipid bilayers, Nanoscale 10 (39) (2018) 18463–18467.
[68] M. Manathunga, X. Yang, M. Olivucci, Electronic state mixing controls the photoreactivity of a rhodopsin with all-trans chromophore analogues, The Journal of Physical Chemistry Letters 9 (21) (2018) 6350–6355.
[69] P.J. Johnson, A. Halpin, T. Morizumi, L.S. Brown, V.I. Prokhorenko, O.P. Ernst, R.J. Dwayne Miller, The photocycle and ultrafast vibrational dynamics of bacteriorhodopsin in lipid nanodiscs, Phys. Chem. Chem. Phys. 16 (39) (2014) 21310–21320.
[70] D. Milic, D.B. Veprintsev, Large-scale production and protein engineering of G protein-coupled receptors for structural studies, Front. Pharmacol. 6 (66) (2015) 66.
[71] J.M. Dörr, S. Scheidelaar, M.C. Koorengevel, J.J. Dominguez, M. Schafer, C.A. van Walree, J.A. Killian, The styrene-maleic acid copolymer: a versatile tool in membrane research, Eur. Biophys. J. 45 (1) (2016) 3–21.